Electron-impact excitation of inelastic transitions in C V

S. S. Tayal
Department of Physics and Astronomy, Louisiana State University, Baton Rouge, Louisiana 70803
(Received 21 April 1986)

The collision strengths for the inelastic transitions among the lowest eleven LS states of C V are presented. Configuration-interaction wave functions are used to represent the eleven target states which are included in the calculation. The calculation for the lower partial waves ($l \leq 11$) are carried out using the R-matrix method. The contribution from higher partial waves is obtained in the close-coupling approximation with exchange terms omitted. The effective collision strengths have been calculated assuming a Maxwellian distribution of electron energies. Results are also presented for calculations in which the five lowest states were included. The present results are compared with the previous calculation of Pradhan, Norcross, and Hummer. Some significant differences are noted, particularly at lower temperatures for some transitions.

I. INTRODUCTION

The knowledge of accurate atomic data such as excitation energies, oscillator strengths, and the excitation rate coefficients for the electron-impact excitation of positive ions is necessary for the better understanding of the physical conditions of astrophysical and laboratory plasmas. Spectral lines of He-like ions have been observed in solar-active regions and flares,[1] and in tokamak plasmas.[2] The resonance, intercombination, and forbidden lines of He-like ions can be used to estimate the electron temperature and density of the plasma.[3,4] The electron-impact excitation of the He-like ions have been previously considered by several authors. Five-state close-coupling calculations have been reported by Van Wyngaarden *et al.*[5] for Li II, C V, O VII, and Si XIII. Nakazaki[6] and Tully[7] carried out Coulomb-Born calculations, while Bhatia and Temkin[8] and McDowell *et al.*[9] used the distorted-wave approximation in their calculation on the He-like ions. These earlier calculations did not take resonance effects into account. The importance of resonance effects for electron-impact excitation of He-like ions have been demonstrated in the recent distorted-wave[10–16] and the R-matrix[17–20] calculations. The resonance effects produce very significant enhancements in the cross sections for most forbidden and semiforbidden transitions and are less important for optically allowed transitions.

Pradhan *et al.*[10,11] carried out distorted-wave calculations for ten inelastic transitions between the five $n=1$ and $n=2$ states in He-like ions: B III, C V, O VII, Ne IX, Si XIII, Ca XIX, and Fe XXV. They used configuration-interaction (CI) wave function for the target representation and included the effects of autoionizing resonances converging to the $n=2$ and $n=3$ states. Steenman-Clark and Faucher[15] also reported the distorted-wave calculations for the $1\,^1S-2\,^3S$ transition in the O VII, Mg XI, Ca XIX, and Fe XXV ions of helium sequence. Faucher and Dubau[16] studied the effect of resonances on the excitation rates of He-like Fe XXV ion. Recently Pradhan[12–14] considered electron-impact excitation of highly charged ions Ca XIX, Fe XXV, Se XXXIII, and Mo XLI using distorted-wave approximation in conjunction with Breit-Pauli approximation to account for the relativistic effects. He found that the resonance, dielectronic, and the intermediate coupling effects are important for these ions. Bednell[21] calculated the collision strengths for transitions between the five lowest states using an equivalent-electron frozen-core approximation for He-like ions between Li II and Fe XXV.

In the earlier R-matrix calculations on electron-impact excitation of He-like O VII and Mg XI ions,[17–20] the accurate collision strengths for several inelastic transitions of astrophysical importance among the lowest eleven target states were reported. In these calculations all the resonances converging to the $n=2$ and $n=3$ levels were taken into account. Doyle *et al.*[22] and Keenan *et al.*[23] used these results to calculate the ratio of the intensity of the forbidden line $1\,^1S-2\,^3S$ to the intercombination line $1\,^1S-2\,^3P^\circ$, which provided an improved estimate of the electron density of the plasma. They also calculated the ratio of the sum of the forbidden and intercombination lines to the resonance line to determine electron temperature. These results were in better agreement with the observations from the sun. In this paper we present the results of our calculations on electron-impact excitation of He-like C V for all transitions between the lowest eleven LS states: $1s^2\,^1S$, $1s2s\,^{1,3}S$, $1s2p\,^{1,3}P^\circ$, $1s3s\,^{1,3}S$, $1s3p\,^{1,3}P^\circ$, and $1s3d\,^{1,3}D$. Some of the preliminary results for $1\,^1S-2\,^3S$ and $1\,^1S-2\,^3P^\circ$ transitions were given in an earlier paper.[18] We used CI target wave functions in our calculations. The lower partial waves corresponding to small values of angular momenta contribute to the collision strengths for forbidden and semiforbidden transitions, while for optically allowed transitions the higher partial waves also make significant contributions to the collision strengths. In order to obtain converged collision strengths for optically allowed transitions, the R-matrix results for lower partial waves are supplemented by higher partial-wave results obtained in close-coupling approximation with exchange effects neglected. The collision

strength for excitation from level i to level f is related to the cross sections σ, in πa_0^2 units by the following relation:

$$\Omega(i \rightarrow f) = \omega_i k_i^2 \sigma(i \rightarrow f) , \quad (1)$$

where ω_i is the statistical weight of level i and k_i^2 is the energy in Rydbergs of the electron relative to level i. The electron collision rates are obtained from collision strengths by integrating over a Maxwell velocity distribution.

II. TARGET WAVE FUNCTIONS

We have generated CI wave functions for the eleven lowest-lying states, $1s^2\,{}^1S$, $1s2s\,{}^{1,3}S$, $1s2p\,{}^{1,3}P^\circ$, $1s3s\,{}^{1,3}S$, $1s3p\,{}^{1,3}P^\circ$, and $1s3d\,{}^{1,3}D$ of C V which are suitable for use in scattering calculations with the R-matrix code.[24] The wave functions were constructed with a common set of radial functions which were chosen to give the best overall representation of the energies of the states. The CI wave function is written in the form

$$\psi(LS) = \sum_{i=1}^{M} a_i \Phi_i(\alpha_i LS) , \quad (2)$$

where each single configuration function Φ_i is constructed from orbitals whose angular momenta are coupled, as specified by α_i, to form a total L and S common to all M configurations. The radial part of each orbital is written in analytic form as a sum of Slater-type orbitals

$$P_{nl} = \sum_{j=1}^{k} C_{jnl} r^{I_{jnl}} \exp(-\xi_{jnl}) . \quad (3)$$

The parameters in Eq. (3) are determined variationally, as discussed by Tayal and Hibbert.[25] Eight orthogonal one-electron orbitals $1s$, $2s$, $2p$, $3s$, $3p$, $3d$, $4s$, and $4p$ were used. The radial function parameters of the $1s$ orbital were taken to be hydrogenic while the other orbitals were determined by minimizing the energies of the states.[26] The values of the Slater-type orbital parameters are listed in Table I. The values of the coefficients C_{jnl} are uniquely determined by the orthonormality conditions. We present the excitation energies obtained in the present calculations in Table II where they are compared with the more accurate theoretical values of Accad *et al.*[27] and Blanchard and Drake.[28] There is normally very good agreement between the two sets of results. However, it may be noted that the present energies for the $1s2s\,{}^1S$ and $1s3s\,{}^1S$ states are not in the correct order. The calculated energies of Accad *et al.*[27] for $1s2s\,{}^1S$ and $1s3s\,{}^1S$ levels are slightly lower than the energies for $1s2p\,{}^3P^\circ$ and $1s3p\,{}^3P^\circ$ levels, respectively. The length and velocity values of oscillator strength for allowed transitions among the target states are presented in Table III. It is clear from the table that the length and velocity values of oscillator strengths agree well with each other and with Schiff *et al.*[29].

III. COLLISION CALCULATION

The wave function describing the C V ion-plus-electron system was expanded as discussed by Burke and Robb.[30] The R-matrix program package described by Berrington *et al.*[24] was used to calculate the $\underline{R}$ matrix on the boundary. A zero logarithmic derivative was imposed at the boundary on the continuum basis orbitals. We have included 25 continuum orbitals of each angular symmetry giving good convergence for energies up to 150 Ry. The number of bound three-electron configurations kept in the R-matrix expansion depends on the total angular momentum (L), spin (S), and parity (π). These configurations were generated by adding the third electron in all possible ways to all configurations that were included in the description of the target states, consistent with the L, S, and π of the state. These calculations are analogous to those for O VII and Mg XI of Kingston and Tayal[17] and Tayal and Kingston,[20] respectively, where further details can be found.

In the outer region where the exchange effects between the scattered electron and the target can be neglected, the coupled integro-differential equations reduce to the set of n-coupled differential equations

$$\left[\frac{d^2}{dr^2} - \frac{l_i(l_i+1)}{r^2} + \frac{2z}{r} + k_i^2\right] u_i(r) = 2\sum_{j=1}^{n} V_{ij}(r) u_j(r), \quad i = 1, \ldots, n \quad (4)$$

where

TABLE I. Values of Slater-type orbital parameters for C V.

I_{jnl}	ξ_{jnl} $2s$	$2p$	$3s$	$3p$	$3d$	$4s$	$4p$
1	3.167 13		6.586 39			6.537 76	
2	2.479 01	2.460 75	3.006 14	4.545 95		3.980 45	4.725 45
3			2.506 35	2.220 21	1.667 52	1.885 05	2.814 24
4						1.950 05	1.768 17

TABLE II. Excitation energies (in a.u.) for the $n=2$ and $n=3$ states in C V relative to the ground state $1\,^1S$.

Index	State	Present calculation	Other calculations
1	$1\,^1S$	0.0	0.0
2	$2\,^3S$	10.9456	10.9854[a]
3	$2\,^3P^\circ$	11.1464	11.1845[a]
4	$2\,^1S$	11.1508	11.1842[a]
5	$2\,^1P^\circ$	11.2784	11.3129[a]
6	$3\,^3S$	12.8962	12.9358[a]
7	$3\,^3P^\circ$	12.9497	12.9895[a]
8	$3\,^1S$	12.9503	12.9884[a]
9	$3\,^3D$	12.9759	13.0161[b]
10	$3\,^1D$	12.9771	13.0171[b]
11	$3\,^1P^\circ$	12.9870	13.0257[a]

[a]Accad *et al.* (Ref. 27).
[b]Blunchard and Drake (Ref. 28).

$$V_{ij}(r)=\frac{N}{r}\delta_{ij}+O(r^{-2})\ . \tag{5}$$

Here N is the number of target electrons. These coupled equations are solved in the outer region and the solutions are matched on the boundary $r=a$ using the $\underline{R}$ matrix which then yield the $\underline{S}$ matrix and hence the collision strengths. In order to include the complicated resonance structures in the cross sections explicitly, we need the solutions of the coupled equations at very fine energy mesh in the threshold energy regions. In practice this is found to be very time consuming. Therefore, we make a simplifying approximation by neglecting higher terms $O(r^{-2})$ in Eq. (5). Now the evaluation of the coupled differential equations reduces to evaluating Coulomb functions on the R-matrix boundary which is computationally much faster and results in massive computer-time savings. We examined the accuracy of this approximation. It is found to give accurate collision strengths for the forbidden transitions. However, for optically allowed transitions the collision strengths may be in error by approximately 5–7%. The solutions satisfying boundary conditions when all channels are open

$$\underline{u}=\underset{\sim}{k}^{-1/2}(\underline{F}+\underline{G}\underline{K}),\quad r\geq a \tag{6}$$

where $\underline{F}$ and $\underline{G}$ are the regular and irregular Coulomb wave functions and $\underline{K}$ is the reactance matrix. We define the $\underline{R}$ matrix on the boundary by

$$\underline{u}=\underline{R}\left[a\frac{d\underline{u}}{dr}-b\underline{u}\right]_{r=a}, \tag{7}$$

where for convenience we have chosen the parameter $b=0$. The $\underline{K}$ matrix can be expressed in terms of the $\underline{R}$ matrix, Coulomb wave functions and their derivatives,[31]

$$\underline{K}^{-1}=-\frac{\underline{G}}{\underline{F}}+\frac{1}{\underline{F}'\underline{F}}-\frac{1}{\underline{\rho}^{1/2}\underline{F}'}\left[\underline{\rho}^{-1}\frac{\underline{F}}{\underline{F}'}-\underline{R}\right]^{-1}\frac{1}{\underline{\rho}^{1/2}\underline{F}'}, \tag{8}$$

where $\underline{\rho}=\underline{k}r$, $\underline{F}'=d\underline{F}/d\underline{\rho}$, and $\underline{G}'=d\underline{G}/d\underline{\rho}$. The $\underline{K}$ matrix is partitioned according to the scheme

$$\underline{K}=\begin{bmatrix}\underline{K}_{oo} & \underline{K}_{oc}\\ \underline{K}_{co} & \underline{K}_{cc}\end{bmatrix}, \tag{9}$$

where o refers to open channels and c to closed channels. The reduced $\underline{K}$ matrix is written as[32]

$$\underline{K}^R=\underline{K}_{oo}-\underline{K}_{oc}[\underline{K}_{cc}+\tan(\pi\nu_c)]^{-1}\underline{K}_{co}\ , \tag{10}$$

where ν_c is the effective quantum number for the closed channels.

TABLE III. Oscillator strengths for electric dipole-allowed transitions in C V.

Transition	Present Calculation f (length)	Present Calculation f (velocity)	Schiff *et al.* (Ref. 29)
$1\,^1S-2\,^1P^\circ$	0.637	0.642	0.647
$1\,^1S-3\,^1P^\circ$	0.120	0.144	0.141
$2\,^1S-2\,^1P^\circ$	0.093	0.096	0.093
$2\,^1S-3\,^1P^\circ$	0.360	0.359	0.352
$2\,^1P^\circ-3\,^1S$	0.021	0.022	0.021
$3\,^1S-3\,^1P^\circ$	0.156	0.158	0.162
$2\,^3S-2\,^3P^\circ$	0.133	0.132	0.131
$2\,^3S-3\,^3P^\circ$	0.310	0.311	0.316
$2\,^3P^\circ-3\,^3S$	0.022	0.022	0.023
$3\,^3S-3\,^3P^\circ$	0.224	0.205	0.220
$2\,^1P^\circ-3\,^1D$	0.710	0.719	
$3\,^1D-3\,^1P^\circ$	0.011	0.011	
$2\,^3P^\circ-3\,^3D$	0.657	0.654	
$3\,^3P^\circ-3\,^3D$	0.048	0.049	

TABLE IV. The collision strengths for electron excitation of the ground $1s^2\,{}^1S$ state ($n=1$) to the $n=2$ states.

Energy	$1\,{}^1S-2\,{}^3S$		$1\,{}^1S-2\,{}^1S$		$1\,{}^1S-2\,{}^3P^\circ$		$1\,{}^1S-2\,{}^1P^\circ$	
(Ry)	11 state	5 state	11 state	5 state	11 state	5 state	11 state	5 state
26.0	0.0068	0.0075	0.0105	0.0102	0.0316	0.0331	0.0390	0.0361
30.0	0.0057	0.0064	0.0109	0.0107	0.0266	0.0285	0.0510	0.0452
50.0	0.0032	0.0030	0.0138	0.0151	0.0128	0.0137	0.0796	0.1066
70.0	0.0020	0.0018	0.0174	0.0197	0.0069	0.0074	0.1269	0.1424
100.0	0.0012	0.0012	0.0217	0.0226	0.0030	0.0035	0.1940	0.1958
110.0	0.0011	0.0011	0.0226	0.0221	0.0025	0.0026	0.2098	0.2120
130.0	0.0008	0.0008	0.0233	0.0213	0.0018	0.0017	0.2284	0.2251
150.0	0.0006	0.0006	0.0224	0.0211	0.0013	0.0012	0.2442	0.2438

The Coulomb functions for open channels are obtained using the computer program of Barnet *et al.*[33] while the computer program of Seaton[34] is used for the Coulomb functions in closed channels. The solutions given by Eqs. (6) and (7) are matched on the boundary $r=a$. The $\underline{K}$ matrix thus obtained at a fine energy mesh are reduced using Eq. (10) to obtain the physical reactance matrix.

We carried out R-matrix calculations for doublet and quartet partial waves of both odd and even parities with total angular momenta from 0 to 11. These partial waves were sufficient to give converged total cross sections for all the spin-changing transitions. For optically allowed transitions the higher partial waves make a significant contribution to the total cross sections, particularly at high energies. The contribution from higher partial waves ($L=12$–30) was obtained in the close-coupling approximation with exchange terms omitted using a noniterative integral equation method (NIEM).[35] The contribution from higher angular momenta ($L=31$ to ∞) was calculated using the Coulomb-Bethe approximation. We repeated the collision calculations with five ($n=1$ and $n=2$) states included in the close-coupling expansion in order to determine the importance of coupling effects to the $n=3$ states.

IV. COLLISION STRENGTHS

The collision calculation was carried out at a very fine energy mesh (0.001 Ry) in the threshold regions. At energies above the highest excitation threshold we encountered the unphysical pseudoresonances in the collision strength resulting from the inclusion of pseudo-orbitals in the target wave functions. The T-matrix smoothing procedure of Burke *et al.*[36] was used to obtain smooth collision strengths in the region of pseudoresonances. The $\underline{T}$ matrices were calculated at a fine mesh covering the energy region where pseudoresonances were present with few energy points both above and below this energy region. Both the real and imaginary parts of the $\underline{T}$ matrices were energy averaged for each partial wave which were then used to obtain collision strengths.

Resonances may contribute substantially to electron collision strengths for some transitions. We have plotted in Figs. 1 and 2 the total collision strengths for the $1\,{}^1S-2\,{}^3S$ and $1\,{}^1S-2\,{}^3P^\circ$ transitions in the energy regions between the $2\,{}^3S$ and $2\,{}^3P^\circ$ and $2\,{}^3P^\circ$ and $2\,{}^1P^\circ$ thresholds, respectively. It is clear from these results that the Rydberg series of resonances play a prominent role in the collision strengths at low electron-impact energies. The resonances have a complicated structure due to several partial waves and series contributing to them. The resonances from higher partial waves are very narrow and do not contribute significantly to the total collision strengths. In Tables IV and V we give the total collision strengths for transitions from the ground $1\,{}^1S$ state to the $2\,{}^{1,3}S$, $2\,{}^{1,3}P^\circ$, $3\,{}^{1,3}S$, $3\,{}^{1,3}P^\circ$ and $3\,{}^{1,3}D$ states at electron energies above the highest excitation threshold. The collision strengths exhibit approximately the expected large-energy behavior. The collision strengths for the spin-changing transitions decrease rapidly with the increase in energy, while the collision strengths for optically allowed

TABLE V. The collision strengths for electron excitation of the ground $1s^2\,{}^1S$ state ($n=1$) to the $n=3$ states.

Energy (Ry)	$1\,{}^1S-3\,{}^3S$	$1\,{}^1S-3\,{}^1S$	$1\,{}^1S-3\,{}^3P^\circ$	$1\,{}^1S-3\,{}^1P^\circ$	$1\,{}^1S-3\,{}^3D$	$1\,{}^1S-3\,{}^1D$
26.0	0.0023	0.0017	0.0085	0.0066	0.0022	0.0009
30.0	0.0018	0.0022	0.0076	0.0097	0.0016	0.0009
50.0	0.0010	0.0026	0.0037	0.0178	0.0006	0.0008
70.0	0.0006	0.0037	0.0021	0.0258	0.0002	0.0012
100.0	0.0004	0.0050	0.0011	0.0412	0.00014	0.0020
110.0	0.0003	0.0052	0.0009	0.0442	0.00014	0.0021
130.0	0.0003	0.0054	0.0006	0.0487	0.00009	0.0022
150.0	0.0002	0.0056	0.0004	0.0557	0.00003	0.0020

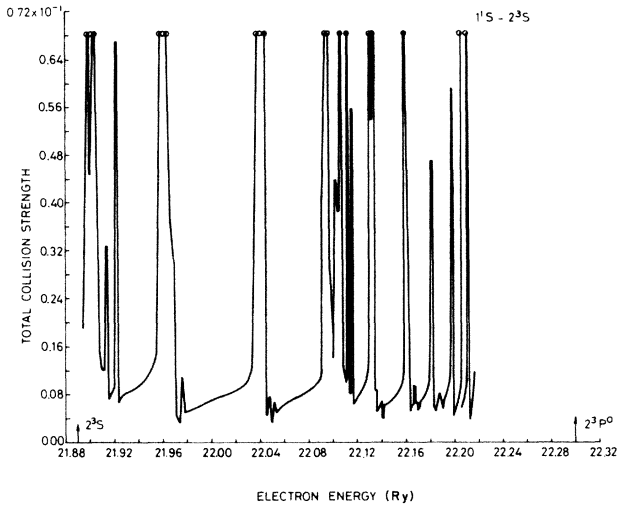

FIG. 1. Electron-collisional excitation $1\,^1S-2\,^3S$ in C v, collision strength in the energy range from the $2\,^3S$ threshold to the $2\,^3P^\circ$ threshold.

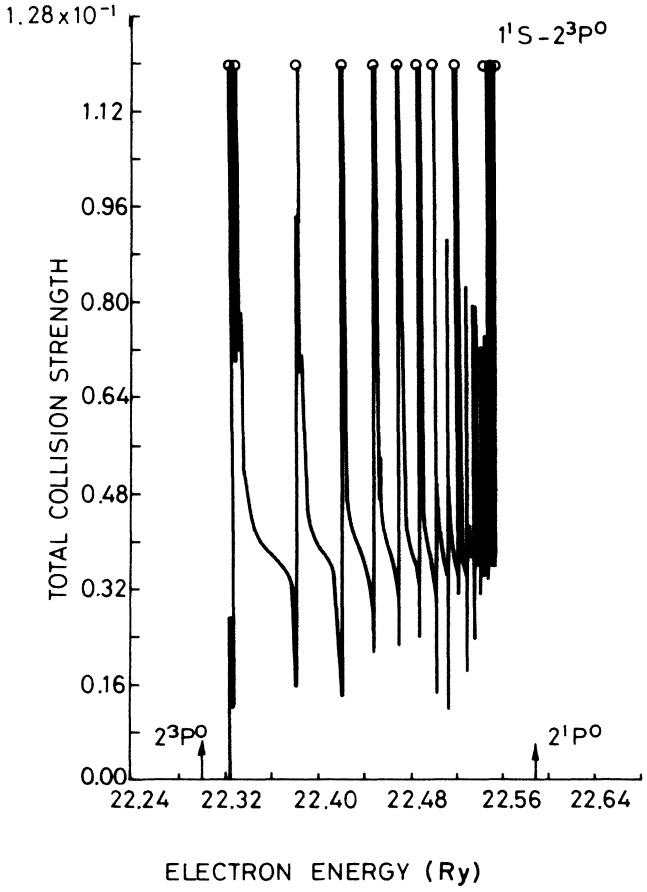

FIG. 2. Electron-collisional excitation $1\,^1S-2\,^3P^\circ$ in C v, collision strength in the energy range from the $2\,^3P^\circ$ threshold to the $2\,^1P^\circ$ threshold.

transitions show approximately $\ln E$ behavior. The total collision strengths for $1\,^1S-2\,^{1,3}S$ and $1\,^1S-2\,^{1,3}P^\circ$ transitions in the energy region above the highest excitation threshold can be compared with the available five-state close-coupling results of Van Wyngerdaan *et al.*[5] and five-state distorted-wave results of Pradhan *et al.*[10] At 110 Ry, the present 11-state and five-state results for $1\,^1S-2\,^{3,1}S$ and $2\,^{3,1}P^\circ$ transitions are in good agreement with each other and also compare well with the corresponding close-coupling results 0.0008, 0.0227, 0.0021, and 0.2049 and distorted-wave values 0.0009, 0.0230, 0.0021, and 0.2001. At 50 Ry, the 11-state results for $1\,^1S-2\,^1S$ and $1\,^1S-2\,^1P^\circ$ transitions are about 25% smaller than the distorted-wave values 0.0185 and 0.1024 and close-coupling results 0.0188 and 0.1110. It may be noted that the collision strengths for $1\,^1S-3\,^3S$ transition are about one-third of the collision strengths for $1\,^1S-2\,^3S$ transition.

V. EFFECTIVE COLLISION STRENGTHS

The electron collision rates are obtained from the collision strengths by integrating over a Maxwell velocity distribution. The effective collision strength from state i to state f is given by

$$\gamma(i\rightarrow f)=\int_0^\infty \Omega(i\rightarrow f)\exp(-E_f/kT_e)d(E_f/kT_e)\ , \tag{11}$$

where E_f is the energy of the incident electron with respect to the excited level, k is the Boltzmann constant, and T_e is the electron temperature in K.

In Table VI we give the effective collision strengths γ

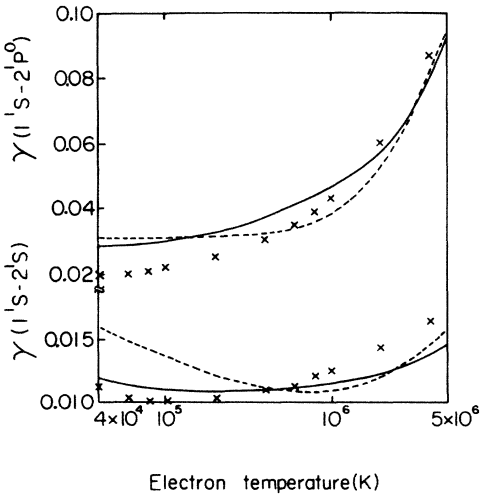

FIG. 3. Electron-collisional strength for the transitions $1\,^1S-2\,^1S$ and $1\,^1S-2\,^1P^\circ$ transitions in C v as a function of electron temperature in K. Solid curve, present 11-state calculation; dashed curve, present five-state calculation; ×, distorted-wave results (Ref. 11).

TABLE VI. Effective collision strengths γ for C V. Numbers in square brackets denote power of ten.

Transition	Electron temperature (10^4 K)										
	4.0	6.0	8.0	10.0	20.0	40.0	60.0	80.0	100.0	200.0	400.0
1-4	1.19[−2]	1.14[−2]	1.12[−2]	1.11[−2]	1.11[−2]	1.12[−2]	1.13[−2]	1.15[−2]	1.16[−2]	1.23[−2]	1.39[−2]
1-5	2.84[−2]	2.90[−2]	2.96[−2]	3.04[−2]	3.34[−2]	3.77[−2]	4.12[−2]	4.41[−2]	4.65[−2]	5.75[−2]	8.10[−2]
1-6	5.29[−3]	4.39[−3]	3.85[−3]	3.51[−3]	2.80[−3]	2.42[−3]	2.21[−3]	2.06[−3]	1.95[−3]	1.59[−3]	1.22[−3]
1-7	1.53[−2]	1.25[−2]	1.12[−2]	1.04[−2]	9.21[−3]	8.48[−3]	7.90[−3]	7.38[−3]	6.95[−3]	5.61[−3]	4.29[−3]
1-8	3.33[−3]	2.71[−3]	2.42[−3]	2.27[−3]	2.06[−3]	2.07[−3]	2.11[−3]	2.14[−3]	2.17[−3]	2.36[−3]	2.81[−3]
1-9	4.40[−3]	3.39[−3]	2.93[−3]	2.68[−3]	2.23[−3]	1.94[−3]	1.77[−3]	1.64[−3]	1.54[−3]	1.21[−3]	8.64[−4]
1-10	2.34[−3]	1.76[−3]	1.49[−3]	1.34[−3]	1.08[−3]	9.58[−4]	9.08[−4]	8.78[−4]	8.58[−4]	8.43[−4]	9.72[−4]
1-11	1.32[−2]	1.02[−2]	9.01[−3]	8.45[−3]	7.97[−3]	8.44[−3]	8.96[−3]	9.45[−3]	9.94[−3]	1.26[−2]	1.80[−2]
2-3	8.16	8.40	8.65	8.90	1.001[1]	1.18[1]	1.32[1]	1.44[1]	1.54[1]	1.89[1]	2.26[1]
2-4	1.06[−1]	1.03[−1]	1.02[−1]	1.03[−1]	1.02[−1]	9.24[−2]	8.25[−2]	7.48[−2]	6.88[−2]	5.12[−2]	3.66[−2]
2-5	1.46[−1]	1.54[−1]	1.64[−1]	1.72[−1]	1.91[−1]	1.76[−1]	1.54[−1]	1.37[−1]	1.23[−1]	8.33[−2]	5.28[−2]
2-6	6.00[−1]	5.20[−1]	4.75[−1]	4.48[−1]	4.09[−1]	4.10[−1]	4.21[−1]	4.31[−1]	4.38[−1]	4.60[−1]	4.81[−1]
2-7	4.66[−1]	3.76[−1]	3.34[−1]	3.13[−1]	2.98[−1]	3.57[−1]	4.28[−1]	4.95[−1]	5.55[−1]	7.93[−1]	1.11
2-8	2.98[−2]	2.27[−2]	1.90[−2]	1.67[−2]	1.20[−2]	8.92[−3]	7.47[−3]	6.54[−3]	5.86[−3]	3.99[−3]	2.59[−3]
2-9	1.10	8.74[−1]	7.86[−1]	7.48[−1]	7.37[−1]	8.08[−1]	8.68[−1]	9.14[−1]	9.49[−1]	1.05	1.11
2-10	1.95[−1]	1.49[−1]	1.28[−1]	1.16[−1]	9.16[−2]	7.36[−2]	6.39[−2]	5.77[−2]	5.33[−2]	4.04[−2]	2.84[−2]
2-11	7.32[−2]	5.49[−2]	4.66[−2]	4.20[−2]	3.27[−2]	2.59[−2]	2.23[−2]	2.00[−2]	1.84[−2]	1.39[−2]	1.04[−2]
3-4	2.66[−1]	2.39[−1]	2.28[−1]	2.24[−1]	2.18[−1]	1.92[−1]	1.67[−1]	1.47[−1]	1.31[−1]	8.82[−2]	5.54[−2]
3-5	8.21[−1]	8.41[−1]	8.80[−1]	9.20[−1]	1.02	9.51[−1]	8.44[−1]	7.55[−1]	6.84[−1]	4.82[−1]	3.19[−1]
3-6	7.97[−1]	6.16[−1]	5.10[−1]	4.42[−2]	3.00[−1]	2.32[−1]	2.18[−1]	2.16[−1]	2.19[−1]	2.52[−1]	3.20[−1]
3-7	3.10	2.48	2.18	2.01	1.74	1.67	1.67	1.68	1.69	1.72	1.75
3-8	1.30[−1]	9.99[−2]	8.37[−2]	7.38[−2]	5.23[−2]	3.80[−2]	3.15[−2]	2.78[−2]	2.53[−2]	1.88[−2]	1.31[−2]
3-9	8.15	6.46	5.79	5.49	5.43	6.21	6.91	7.46	7.91	9.17	9.86
3-10	8.38[−1]	6.38[−1]	5.42[−1]	4.87[−1]	3.73[−1]	2.89[−1]	2.46[−1]	2.21[−1]	2.03[−1]	1.55[−1]	1.09[−1]
3-11	3.59[−1]	2.67[−1]	2.25[−1]	2.02[−1]	1.54[−1]	1.21[−1]	1.04[−1]	9.34[−2]	8.63[−2]	6.63[−2]	4.71[−2]
4-5	3.49	3.60	3.72	3.83	4.33	5.11	5.73	6.23	6.65	8.06	9.46
4-6	6.37[−1]	4.90[−2]	4.03[−2]	3.46[−2]	2.21[−2]	1.46[−2]	1.17[−2]	1.00[−2]	8.93[−3]	6.25[−3]	4.19[−3]

TABLE VI. (*Continued*).

Transition	Electron temperature (10^4 K)										
	4.0	6.0	8.0	10.0	20.0	40.0	60.0	80.0	100.0	200.0	400.0
4-7	9.65[−2]	7.56[−2]	6.45[−2]	5.77[−2]	4.30[−2]	3.24[−2]	2.72[−2]	2.41[−2]	2.20[−1]	1.63[−2]	1.13[−2]
4-8	2.29[−1]	1.88[−1]	1.70[−1]	1.61[−1]	1.51[−1]	1.57[−1]	1.64[−1]	1.69[−1]	1.73[−1]	1.84[−1]	1.94[−1]
4-9	2.17[−1]	1.66[−1]	1.42[−1]	1.29[−1]	1.01[−1]	8.05[−2]	6.96[−2]	6.27[−2]	5.78[−2]	4.38[−2]	3.06[−2]
4-10	4.05[−1]	3.20[−1]	2.85[−1]	2.69[−1]	2.54[−1]	2.62[−1]	2.68[−1]	2.72[−1]	2.75[−1]	3.00[−1]	3.57[−1]
4-11	1.88[−1]	1.43[−1]	1.24[−1]	1.15[−1]	1.08[−1]	1.25[−1]	1.44[−1]	1.63[−1]	1.81[−1]	2.63[−1]	4.08[−1]
5-6	2.41[−1]	1.86[−1]	1.54[−1]	1.33[−1]	8.49[−2]	5.53[−2]	4.34[−2]	3.68[−2]	3.25[−2]	2.25[−2]	1.50[−2]
5-7	4.38[−1]	3.39[−1]	2.86[−1]	2.54[−1]	1.84[−1]	1.36[−1]	1.15[−1]	1.02[−1]	9.28[−2]	6.98[−2]	4.91[−2]
5-8	8.92[−2]	6.82[−2]	5.76[−2]	5.15[−2]	4.17[−2]	4.25[−2]	4.70[−2]	5.17[−2]	5.61[−2]	7.47[−2]	1.02[−1]
5-9	9.48[−1]	7.23[−1]	6.15[−1]	5.52[−1]	4.22[−1]	3.26[−1]	2.78[−1]	2.48[−1]	2.28[−1]	1.74[−1]	1.23[−1]
5-10	3.39	2.65	2.34	2.19	2.03	2.10	2.18	2.23	2.28	2.51	2.92
5-11	8.44[−1]	6.54[−1]	5.79[−1]	5.45[−1]	5.16[−1]	5.41[−1]	5.63[−1]	5.77[−1]	5.85[−1]	6.05[−1]	6.32[−1]
6-7	7.74[1]	6.63[1]	6.25[1]	6.18[1]	6.87[1]	8.58[1]	9.98[1]	1.11[2]	1.21[2]	1.50[2]	1.76[2]
6-8	3.53[−1]	2.71[−1]	2.27[−1]	1.99[−1]	1.38[−1]	1.00[−1]	8.48[−2]	7.64[−2]	7.09[−2]	5.67[−2]	4.39[−2]
6-9	1.02[1]	7.94	6.98	6.49	5.81	5.63	5.56	5.49	5.42	5.07	4.48
6-10	6.80[−1]	5.08[−1]	4.22[−1]	3.70[−1]	2.58[−1]	1.80[−1]	1.46[−1]	1.28[−1]	1.17[−1]	9.05[−2]	6.60[−2]
6-11	3.86[−1]	2.84[−1]	2.35[−1]	2.06[−1]	1.47[−1]	1.05[−1]	8.70[−2]	7.69[−2]	7.06[−2]	5.48[−2]	3.97[−2]
7-8	5.17[−1]	3.92[−1]	3.24[−1]	2.81[−1]	1.87[−1]	1.26[−1]	1.00[−1]	8.72[−2]	7.86[−2]	5.83[−2]	4.11[−2]
7-9	1.34[2]	1.05[2]	9.28[1]	8.68[1]	7.88[1]	7.64[1]	7.47[1]	7.29[1]	7.12[1]	6.32[1]	5.18[1]
7-10	2.39	1.78	1.47	1.29	8.85[−1]	6.11[−1]	4.94[−1]	4.32[−1]	3.95[−1]	3.07[−1]	2.25[−1]
7-11	2.10	1.54	1.27	1.11	7.84[−1]	5.69[−1]	4.77[−1]	4.28[−1]	3.96[−1]	3.17[−1]	2.41[−1]
8-9	7.51[−1]	5.59[−1]	4.63[−1]	4.04[−1]	2.77[−1]	1.91[−1]	1.54[−1]	1.34[−1]	1.22[−1]	9.44[−2]	6.89[−2]
8-10	2.97	2.32	2.04	1.90	1.72	1.70	1.70	1.69	1.68	1.64	1.57
8-11	3.79[1]	3.00[1]	2.73[1]	2.65[1]	2.81[1]	3.37[1]	3.84[1]	4.23[1]	4.55[1]	5.55[1]	6.42[1]
9-10	8.38	6.25	5.18	4.53	3.15	2.21	1.81	1.60	1.48	1.17	8.78[−1]
9-11	2.43	1.77	1.46	1.27	8.71[−1]	6.02[−1]	4.87[−1]	4.27[−1]	3.91[−1]	3.06[−1]	2.25[−1]
10-11	7.54[1]	5.86[1]	5.20[1]	4.92[1]	4.75[1]	5.14[1]	5.50[1]	5.79[1]	6.03[1]	6.76[1]	7.34[1]

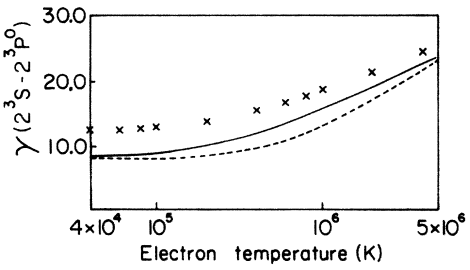

FIG. 4. The curves are the same as for Fig. 3, but for the transition $2\,^3S-2\,^3P^\circ$ in C V.

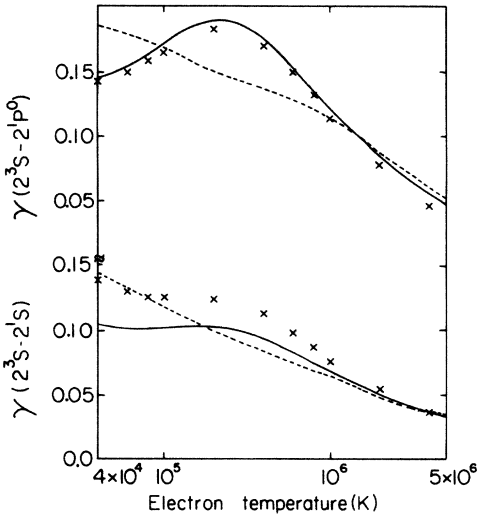

FIG. 5. The curves are the same as for Fig. 3, but for the transitions $2\,^3S-2\,^1S$ and $2\,^3S-2\,^1P^\circ$ in C V.

for the forbidden, intercombination, and allowed transitions over a wide temperature range 4×10^4–4×10^6 K. The keys of the states for the transitions are given in Table II. The effective collision strengths for $1\,^1S-2\,^3S$ and $1\,^1S-2\,^3P^\circ$ transitions are not included in these tables, as these were given in a previous paper.[18] In order to compare the present 11- and five-state results with the previously available distorted-wave results of Pradhan *et al.*,[11] we have plotted γ against the electron temperature T_e in Figs. 3, 4, and 5. The present 11- and five-state results are shown by solid and dashed lines, respectively, while the distorted-wave values are indicated by crosses. For $1\,^1S-2\,^1S$ and $2\,^1P^\circ$ transitions (Fig. 3) the distorted-wave results of Pradhan *et al.* are lower than the present 11-state and five-state results at low temperatures and becomes larger at higher temperatures. The five-state results are considerably higher than the eleven-state results at lower temperatures for the $1\,^1S-2\,^1S$ transition. It is clear from Fig. 4 that the distorted-wave results are larger as compared to the present 11-state and five-state results for the allowed $2\,^3S-2\,^3P^\circ$ transition. The effective collision strengths for the $2\,^3S-2\,^1P^\circ$ transition obtained in the 11-state and distorted-wave calculations are in good agreement over the entire temperature range. However, the five-state results show significant differences. The five-state results lie below the 11-state results in the temperature range 10^5–10^6 K. A part of the discrepancy is due to the absence of the $1s\,3lnl'$ group of resonances in the five-state calculation. For $2\,^3S-2\,^1S$ transition, the three sets of calculations differ significantly at lower temperatures while at higher temperatures ($>10^6$ K) they are in good agreement. The five-state results are normally larger than the 11-state values at lower energies. This is due to the fact that the $1s\,2lnl'$ series of resonances in the five-state results are larger than the corresponding $1s\,2lnl'$ resonances occurring in the 11-state calculations.[20] At higher energies the differences between the 11- and five-state results is perhaps due to the better target wave functions used in the 11-state calculations.

In this paper we have presented collision strengths and effective collision strengths for several transitions obtained in 11- and five-state R-matrix calculations. Configuration interaction wave functions are used to represent the target states. The 11-state calculation includes $1s\,2lnl'$ and $1s\,3lnl'$ groups of resonances and these are found to make significant enhancements in the collision strengths for some transitions. The present results differ significantly from the previous distorted-wave calculation of Pradhan *et al.* for some transitions, particularly at low incident electron energies.

ACKNOWLEDGMENTS

The author is grateful to Dr. Ronald J. W. Henry for providing the research facilities. This work is supported in part by the U.S. Department of Energy (Division of Chemical Sciences).

[1]D. L. McKenzie, R. M. Brussard, P. B. Landecker, H. R. Rugge, R. M. Young, G. A. Doschek, and U. Feldman, Astrophys. J. **238**, L43 (1980).
[2]TFR Group, J. G. Doyle, and J. L. Schwob, J. Phys. B **15**, 813 (1982).
[3]A. H. Gabriel and C. Jordan, Mon. Not. R. Astron. Soc. **145**, 241 (1969).
[4]G. R. Blumenthal, G. W. F. Drake, and W. H. Tucker, Astrophys. J. **172**, 205 (1972).
[5]W. L. Van Wyngaarden, K. Bhadra, and R. J. W. Henry, Phys. Rev. A **20**, 1409 (1979).
[6]S. Nakazaki, J. Phys. Soc. Jpn. **41**, 2084 (1976).
[7]J. A. Tully, J. Phys. B **7**, 386 (1974).
[8]A. K. Bhatia and A. Temkin, J. Phys. B **10**, 2893 (1977).
[9]M. R. C. McDowell, L. A. Morgan, V. P. Myerscough, and T. Scott, J. Phys. B **10**, 2727 (1977).
[10]A. K. Pradhan, D. W. Norcross, and D. G. Hummer, Phys. Rev. A **23**, 619 (1981).
[11]A. K. Pradhan, D. W. Norcross, and D. G. Hummer, Astrophys. J **246**, 1031 (1981).
[12]A. K. Pradhan, Phys. Rev. A **28**, 2113 (1983).
[13]A. K. Pradhan, Phys. Rev. A **28**, 2128 (1983).
[14]A. K. Pradhan, Phys. Rev. A **30**, 100 (1984).
[15]L. Steenman-Clark and P. Faucher, J. Phys. B **17**, 73 (1984).

[16]P. Faucher and J. Dubau, Phys. Rev. A **31**, 3672 (1985).
[17]A. E. Kingston and S. S. Tayal, J. Phys. B **16**, 3465 (1983).
[18]S. S. Tayal and A. E. Kingston, J. Phys. B **17**, L145 (1984).
[19]S. S. Tayal and A. E. Kingston, J. Phys. B **17**, 1383 (1984).
[20]S. S. Tayal and A. E. Kingston, J. Phys. B **18**, 2983 (1985).
[21]N. R. Badnell, J. Phys. B **18**, 955 (1985).
[22]J. G. Doyle, S. S. Tayal, and A. E. Kingston, Mon. Not. R. Astron. Soc. **203**, 31P (1983).
[23]F. P. Keenan, S. S. Tayal, and A. E. Kingston, Mon. Not. R. Astron. Soc. **207**, 51P (1984).
[24]K. A. Berrington, P. G. Burke, M. Le Dourneuf, W. D. Robb, K. T. Taylor, and Vo Kylan, Comput. Phys. Commun. **14**, 367 (1978).
[25]S. S. Tayal and A. Hibbert, J. Phys. B **17**, 3835 (1984).
[26]A. Hibbert, Comput. Phys. Commun. **9**, 141 (1975).
[27]Y. Accad, C. L. Perkeris, and B. Schiff, Phys. Rev. A **11**, 1479 (1975).
[28]P. Blanchard and G. W. F. Drake, J. Phys. B. **6**, 2495 (1973).
[29]B. Schiff, C. L. Pekeris, and Y. Accad, Phys. Rev. A **4**, 885 (1971).
[30]P. G. Burke and W. D. Robb, Adv. At. Mol. Phys. **11**, 143 (1975).
[31]M. Gailitis, Zh. Eksp. Teor. Fiz. **44**, 1974 (1963) [Sov. Phys.—JETP **17**, 1328 (1963)].
[32]M. J. Seaton, Rep. Prog. Phys. **46**, 167 (1983).
[33]A. R. Barnet, D. H. Feng, J. W. Steed, and L. J. B. Goldfarb, Comput. Phys. Commun. **8**, 377 (1974).
[34]M. J. Seaton, Comput. Phys. Commun. **25**, 87 (1982).
[35]R. J. W. Henry, S. P. Rountree, and E. R. Smith, Comput. Phys. Commun. **23**, 233 (1981).
[36]P. G. Burke, K. A. Berrington, and C. V. Sukumar, J. Phys. B **14**, 289 (1981).